Schweizerische Eidgenossenschaft
Confédération suisse
Confederazione Svizzera
Confederaziun svizra

Eidgenössisches Departement des Innern EDI
Bundesamt für Meteorologie und Klimatologie MeteoSchweiz

Data quality monitoring with Pyrad

Overview

	In progress	In validation	Approved
Document status	☒	☐	☐

Version 0.5

Document History

Responsible People

Creation/Edition	Jordi Figueras i Ventura (fvj)
Revision	MALSPLUS team
Approval	MDR
Further information	Pyrad users

Version Control

Version	**Edited by**	**Date**	**Activity**
0.1	fvj	13.04.2017	Creation
0.2	fvj	11.09.2017	References added. Minor corrections
0.3	fvj	15.09.2017	Added description of monitoring alarms
0.4	fvj	29.09.2017	Added ZDR monitoring in snow and with vertically pointing antenna. Minor corrections
0.5	fvj	20.03.2018	Added description of ground clutter monitoring and specific information for C-band network data. Changes in the description of some algorithms. Update of the plot examples

Contents

Figures

Tables

Chapter 1 Introduction

This document is meant to provide an overview of the various data quality monitoring techniques implemented using the Pyrad processing framework. Pyrad is an open source program, written in Python, aimed at processing polar radar data. The Pyrad program is used for the operational data processing and data quality monitoring of the armasuisse owned and MeteoSwiss operated METEOR 50DX and for the data quality monitoring of the MeteoSwiss C-band radar network. The Pyrad documentation can be found in https://github.com/meteoswiss-mdr/pyrad/tree/master/doc.

The focus of this document is to present the different monitoring techniques implemented in Pyrad and discuss its methodology. The document is structured as follows: Chapter 2 describes the required data pre-processing in order to obtain the variables to be analyzed for the METEOR 50DX and the Operational C-band network, chapter 3 discusses several methods to monitor the quality of the polarimetric variables, chapter 4 describes the methodology used for the inter-comparison between radars while chapter 5 describes the monitoring of the receiver and the antenna using sun hits.

Chapter 2 Pre-processing

2.1 METEOR 50DX data pre-processing

2.1.1 Input data

The METEOR 50DX can provide all the polarimetric and Doppler moments of a STAR (Simultaneous Transmission And Reception) system in two forms, either with a user defined Doppler spectra filtering window or without any filtering. The data is stored in the SELEX proprietary Rainbow file format. For most applications, except for the sun measurements, filtered data is used. The data used in the pre-processing is the horizontal reflectivity (Z_h), the vertical reflectivity (Z_v) the differential reflectivity (Z_{dr}), the co-polar correlation coefficient (ρ_{hv}), the raw differential phase shift (ψ_{dp}), the differential phase shift on propagation as processed by the Rainbow processor (ϕ_{dp}) and the specific differential phase (K_{dp}).

In addition to the radar data, the auxiliary data used is the 3D temperature field from the COSMO model (T) in Swiss coordinates at hourly temporal resolution and a visibility map VIS (in antenna coordinates) pre-computed from Digital Elevation Models (DEM). Visibility data can be obtained from a separate IDL software developed in-house called gecs [1].

2.1.2 General processing flow

Fig. 1 shows the pre-processing flow diagram for the METEOR 50DX. Temperature from the COSMO model is converted into antenna coordinates using a nearest neighbor interpolation method. The indices of the 3D COSMO data corresponding to each range gate can either be obtained from the radar volume while processing or computed offline taking a radar volume with similar characteristics as reference. If the radar scans are fairly similar between them, the off-line computation is preferred in order to speed up the processing. If the COSMO indices are pre-computed and the radar volume may vary from one scan to the next another nearest neighbor interpolation is performed.

The first step in the pre-processing is the creation of a dynamic clutter map (Clutter ID in Fig. 1). This is performed for each radar volume by computing the textures (local standard deviation) of ρ_{hv}, ψ_{dp}, Z_{dr} and Z_h and the value of ρ_{hv}. The texture is computed along the ray using a window of a predefined width. The width of the window is a tradeoff between having enough samples to smooth the influence of noise in the signals and having a homogeneous field. If the computed textures exceed predefined thresholds or ρ_{hv} is below a predefined value the gate is labeled as clutter (a value of 2). If the Z_h value is not a valid number the gate is labeled as noise (a value of 1). Otherwise it is labeled as precipitation (value of 3). Table 1 shows the values used in the clutter identification algorithm. This values were defined as a result of a sensitivity analysis.

The second step is to suppress the gates containing clutter (mask the array) on all the variables that are going to be used in the data quality monitoring, i.e. Z_h, Z_v, Z_{dr}, ρ_{hv}, ϕ_{dp} and K_{dp} (Clutter Suppression in Fig. 1). It follows a suppression of significantly blocked (less than 90% visibility according to DEM simulations) gates (Vis filter in Fig. 1). Such threshold guaranties that the polarimetric variables are virtually unaffected by beam blockage.

Table 1 Values used in the clutter identification algorithm

Keyword	Value	Unit
$wind$	7	gates
ρ_{hv}^{min}	0.6	-
$\sigma_{\phi_{dp}}^{max}$	20	°
$\sigma_{\rho_{hv}}^{max}$	0.3	-
$\sigma_{Z_h}^{max}$	8	dBZ
$\sigma_{Z_{dr}}^{max}$	2.85	dB

Z_h and Z_{dr} are corrected for attenuation using the ZPhi algorithm [2] to estimate the attenuation, which uses the total span of ϕ_{dp} at the end of the ray. The attenuation is estimated up to the iso-0° (first 0 cross according to the COSMO temperature estimate).

Finally an hydrometeor classification is produced using corrected Z_h, Z_{dr}, ρ_{hv} and K_{dp} and the temperature using the semi-supervised approach described in [3].

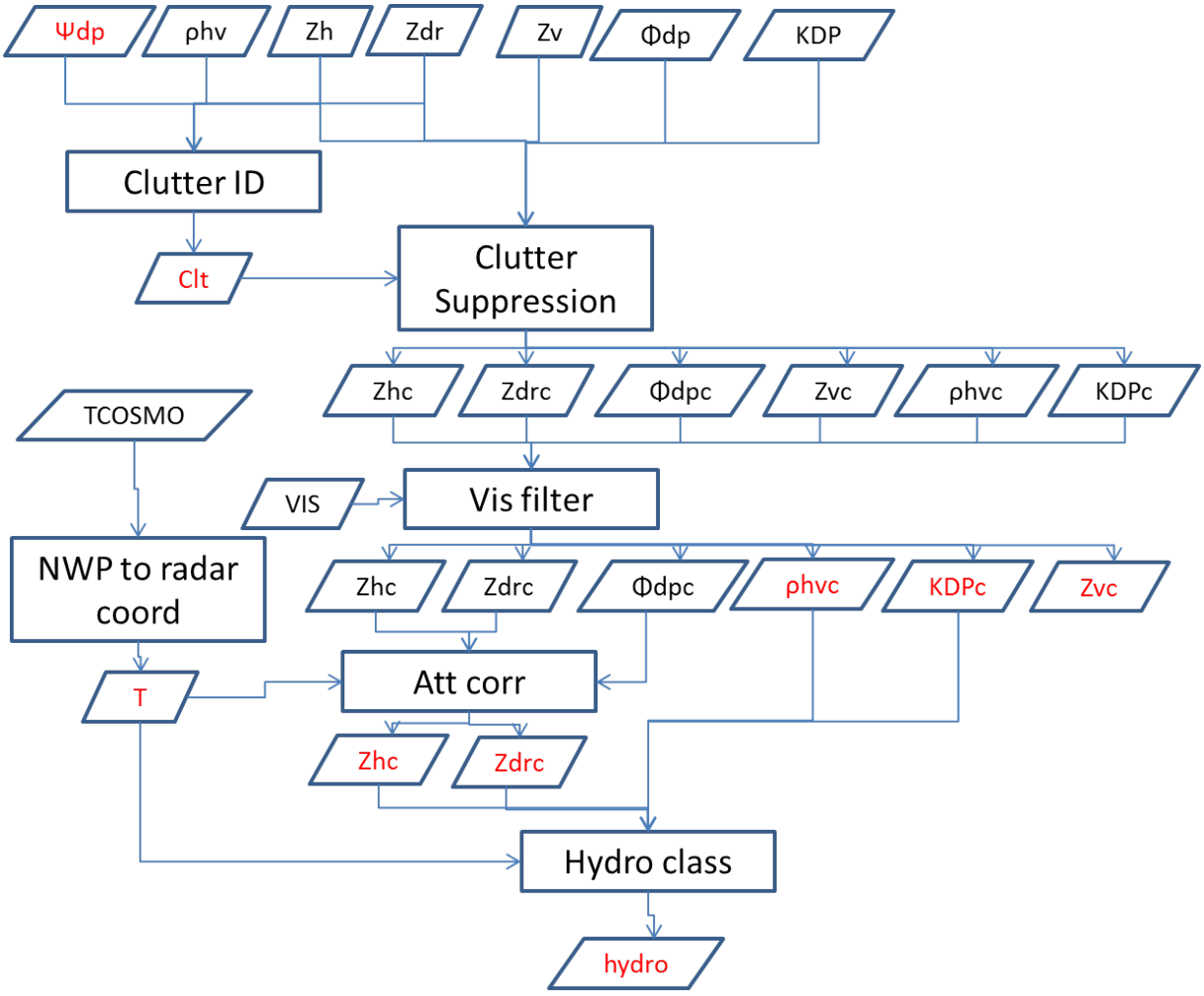

Fig. 1 Flow diagram of the METEOR 50DX pre-processing for data quality monitoring. Variables in red are those used in the monitoring algorithms. The suffix "c" denotes that the variable has undergone a correction respect to the original value

2.1.3 Processing flow for clutter monitoring

Fig. 2 shows the pre-processing flow diagram for the monitoring of the reflectivity stability using clutter with the METEOR 50DX. The basic step is to identify clutter gates using the method explained in the previous section and then filter out all non-clutter reflectivity gates. This processing is performed over the three lowest elevations (3°, 4°, 5.7°) up to 10 km. the variables used are those where no Doppler clutter filtering has been performed.

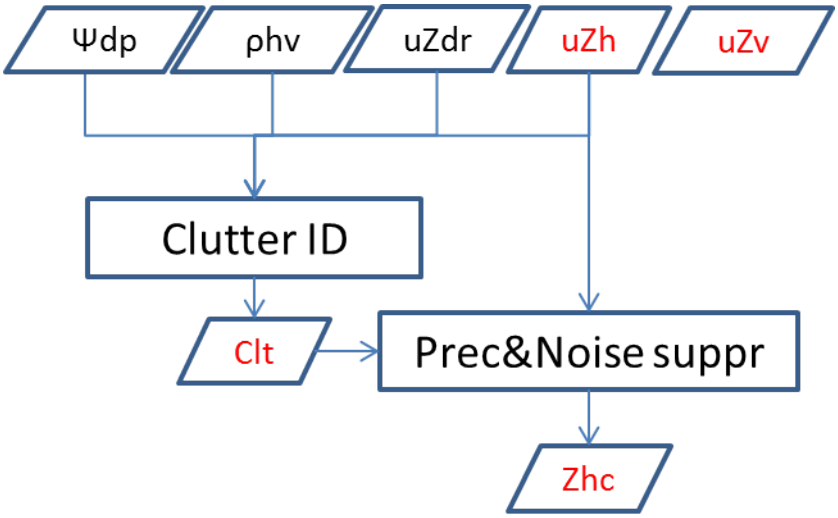

Fig. 2 Flow diagram of the METEOR 50DX pre-processing for ground clutter monitoring. Variables in red are those used in the monitoring algorithms.

2.2 Operational C-band network data pre-processing

2.2.1 Input data

C-band radars basic output are the polarimetric and Doppler moments at high resolution (83 m). They are stored in Eldes proprietary METRANET format. A Centralized Computing System performs the clutter identification and suppression and reduces the resolution to 500 m. The low resolution output is the one used to derive all the operational products, including the data quality monitoring.

Operationally, no Doppler spectra filtering is applied on the data. Moreover, when computing the co-polar correlation coefficient the noise power is not subtracted from the signal. We call the uncorrected variable ρ_{hv}^{u}. The noise correction has to be performed at pre-processing time and for that the noise power at the horizontal and vertical channels (N_h and N_v) is required. Furthermore, no processing of the raw differential phase shift ψ_{dp} is performed operationally and therefore it also has to be performed at pre-processing time.

Summarizing the input radar variables of the processing are Z_h, Z_v, Z_{dr}, ρ_{hv}^{u}, ψ_{dp}, N_h and N_v. As for the METEOR 50DX data processing temperature from the COSMO model and a visibility map are also used in the processing.

2.2.2 Optimal processing flow

Fig. 3 summarizes the pre-processing flow diagram for the operational C-band radar network. The first correction performed is to correct for the noise ρ_{hv}^{u} using N_h and N_v and Z_{dr} as follows [4]:

$$\rho_{hv} = \sqrt{\left(1 + \frac{1}{snr_h}\right)\left(1 + \frac{Z_{dr}^{lin}}{\alpha \cdot snr_h}\right)}$$

Where Z_{dr}^{lin} is the differential reflectivity in linear units, snr_h is the horizontal channel signal to noise ratio in linear units and:

$$\alpha = \frac{n_h}{n_v}$$

is the channel imbalance, where the noise power is in linear units. It should be noticed that the noise level is estimated from data taken at 35° or 40° elevation and at far range in order to minimize the influence of possible radar echoes. This may result on an underestimation of the noise, particularly at low elevations where thermal noise from emissions of the surrounding orography may increase the noise floor. As it is the case for the METEOR 50DX data after a clutter identification a clutter suppression and visibility filtering follows. The filtering is applied to Z_h, Z_v, Z_{dr}, ρ_{hv} and ψ_{dp}.

Unlike with the METEOR 50DX, ψ_{dpc} requires further processing since it is not performed operationally. The first step is to further filter it for SNR according to a prescribed SNR threshold to minimize the influence of phase noise (currently set to 10 dB). The result is then input into a function that performs two steps:

- **The first step is to estimate the system differential phase shift** using the technique described in section 3.1 and correct for it. If no system phase shift has been determined for a particular ray but there are rays in the sweep where a system phase shift has been identified, the median of those rays is taken as the ray phase shift. If no phase shift has been identified, the median of the differential phase is taken as the system phase shift. If there is no differential phase data in the sweep the system phase shift is set to 0.

- **In the second step a median moving filter with two window lengths is applied** according to a threshold on reflectivity Z_{th}. The short one r_s^{wind} is applied to high reflectivity gates whereas the long one r_l^{wind} is applied to low reflectivity gates. In this way, a better filtering of the phase noise is performed to weak homogeneous signals while keeping a good spatial resolution on small but intense precipitation cells, where the spatial variability of precipitation is higher

The resultant ϕ_{dp} is used in the attenuation correction up to the 0°C isotherm using the ZPhi algorithm as in the case of the METEOR 50DX data. From ϕ_{dp} K_{dp} is estimated using a least square regression with again two different windows, typically using the same criteria as for the Φ_{dp} smoothing.

As for the METEOR 50DX data, an hydrometeor classification is produced using corrected Z_h, Z_{dr}, ρ_{hv} and K_{dp} and the temperature.

Table 2 Parameters used for the C-band radars Φ_{dp} smoothing

Keyword	Value	Unit
r_{min}	1000	m
r_{max}	50000	m
r_{cell}	1000	m
Z_{min}	20	dBZ
Z_{max}	40	dBZ
r_s^{wind}	1000.	km
r_l^{wind}	3000.	km
Z_{th}	40	dBZ

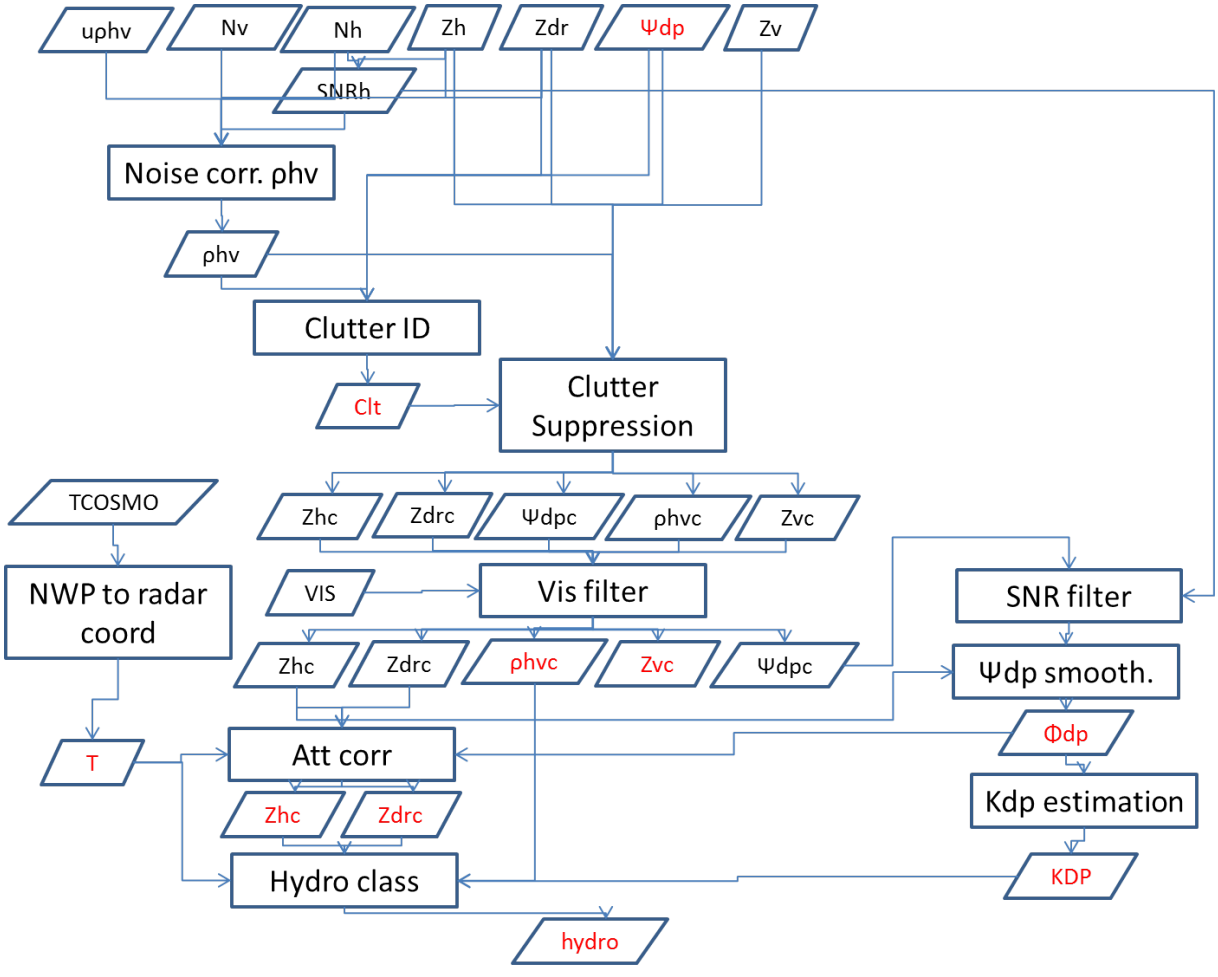

Fig. 3 Flow diagram of the operational C-band radars pre-processing for data quality monitoring. Variables in red are final products used in the monitoring algorithms. The suffix "c" denotes that the variable has undergone a correction respect to the original value

2.2.3 Operational processing flow

Due to the long computation time required to process the data in an optimal way a simplified processing respect to the one described in section 2.2.2 has been implemented operationally. 3 different data processing routines are used: one for the monitoring of the polarimetric data, one for the inter-comparison between radars and one for the monitoring using ground clutter.

Fig. 4 shows the flow diagram of the pre-processing used for the monitoring of the polarimetric variables. It essentially consists on obtaining the height of the range gate with respect to the iso-0° isotherm (HZT) coming from the Numerical Weather Prediction model (NWP), computing the SNR of the horizontal channel and subtracting the estimated system differential phase from the raw differential phase. The parameters used to correct Φ_{dp} can be seen in Table 3. The whole processing is done up to 50 km from the radar.

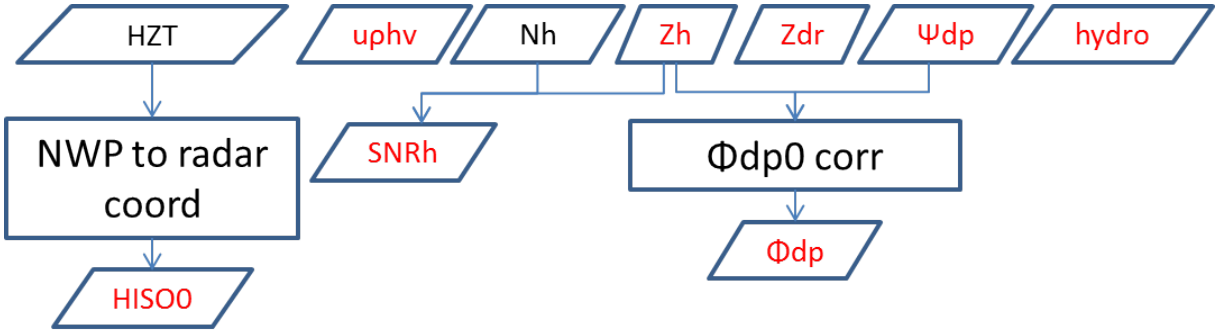

Fig. 4 Flow diagram of the operational C-band radars pre-processing for polarimetric data quality monitoring. Variables in red are final products used in the monitoring algorithms.

Table 3 Parameters used for the C-band radars Φ_{dp} offset correction

Keyword	Value	Unit
r_{min}	1000	m
r_{max}	50000	m
r_{cell}	1000	m
Z_{min}	20	dBZ
Z_{max}	40	dBZ

Fig. 5 shows the flow diagram of the pre-processing used for the intercomparison between radars. As with the monitoring of polarimetric variables, it also consists on obtaining the height of the range gate with respect to the iso-0° and subtracting the estimated system differential phase from the raw differential phase but the processing is performed up to a distance of 150 km from the radar and involves only the 12 lowest elevations.

Fig. 6 shows the flow diagram of the pre-processing used for the monitoring of ground clutter. It uses the high resolution (83 m) data and processes the 3 lowest elevations up to 10 km from the radar. One step is to re-map the operational clutter exit code to the clutter echo id used in Pyrad.

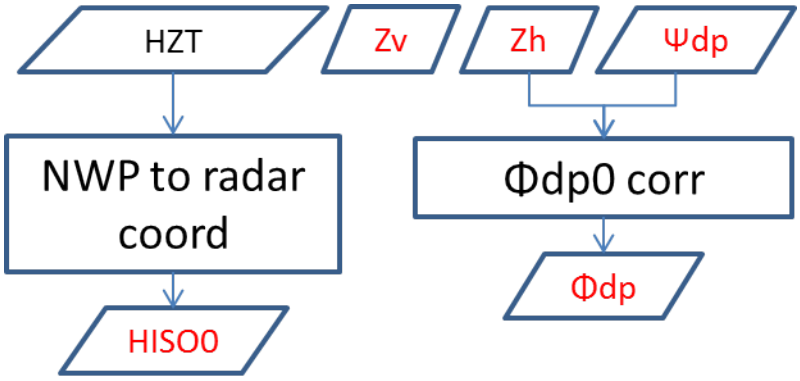

Fig. 5 Flow diagram of the operational C-band radars pre-processing for radar inter-comparison. Variables in red are final products used in the monitoring algorithms

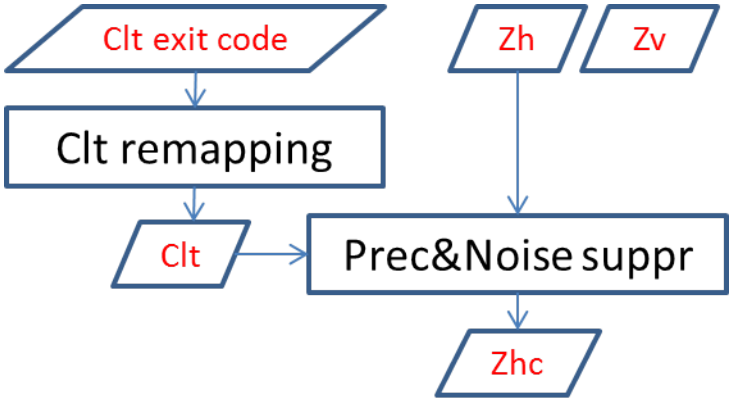

Fig. 6 Flow diagram of the operational C-band radars pre-processing for ground clutter monitoring. Variables in red are final products used in the monitoring algorithms

Chapter 3 Polarimetric data quality monitoring

The polarimetric data quality monitoring is performed by providing properly filtered data to the function process_monitoring, which essentially computes a histogram of the data at each ray. Further details on the various data quality indicators can be found in [5]. Instantaneous histograms provide the basis for the products that show the evolution of the data on a scan by scan basis. The instantaneous histograms get also accumulated over a period of time. The accumulated histogram provides the basis for the daily analysis of the data quality, as further explained in section 3.6.

3.1 System differential phase shift estimation

The system differential phase shift (ϕ_{dp0}) provides an indication of hardware variations in the receiver or transmitter path. If there is no hardware change, it is expected to be constant over time. Ideally, it should be a single value for each radar but it is known that nearby obstacles, and in particular the radome may cause spatial variations.

The flow diagram of the ϕ_{dp0} estimation can be seen in Fig. 7. The estimation of $\phi_{dp0}$is performed on a ray basis. The first step is to identify the precipitation cell closest to the radar. The search of the precipitating cell is performed within a user defined range delimited by r_{min} and r_{max}. The minimum range is chosen in order to avoid the effects of the TR limiter, residual clutter, etc. while the maximum range is imposed to ensure high signal to noise ratio and avoid issues such as partial beam filling. The precipitation cells are identified by looking for profiles of reflectivity with reflectivity within predefined values Z_{min} and Z_{max}. The minimum and maximum values are defined in order to keep a high SNR and at the same time to avoid possible contamination by residual clutter or hail. If a suitable cell with a minimum extension given by r_{cell} is identified, the average in sine and cosine is computed as:

$$\phi_{dp0} = \tan^{-1}\left(\frac{\sum_{\forall i}\sin\phi_{dp}[i]}{\sum_{\forall i}\cos\phi_{dp}[i]}\right)$$

Where the index i runs along the length of the precipitation cell. Although a single value per ray is obtained, for practical reasons the same value is stored in all the gates of such ray. Table 4 summarizes the parameters used for the ϕ_{dp0} estimation of the various radars.

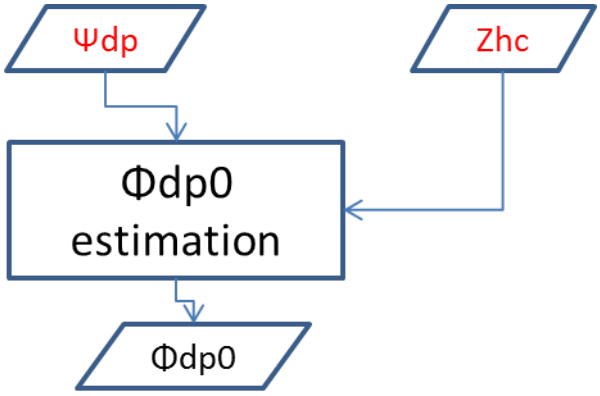

Fig. 7 Φ_{dp} offset estimation flow diagram

Table 4 Parameters used for the METEOR 50DX and the C-band radars Φ_{dp} offset estimation.

Keyword	Value	Unit
r_{min}	1000	m
r_{max}	50000	m
r_{cell}	1000	m
Z_{min}	20	dBZ
Z_{max}	40	dBZ

3.2 Co-polar correlation coefficient in rain

The co-polar correlation coefficient in rain is linked to the quality of the antenna and how well the horizontal and vertical polarization antenna diagrams match. In pure rain, a rather high value (on the order of 0.997) is expected.

Fig. 8 shows a flow diagram of ρ_{hv} estimation in rain. The estimation is performed over data fulfilling the following criteria: It is within a range delimited by r_{min} and r_{max}, the reflectivity is within Z_{min} and Z_{max} values and it is below the melting layer by a sufficiently large margin.

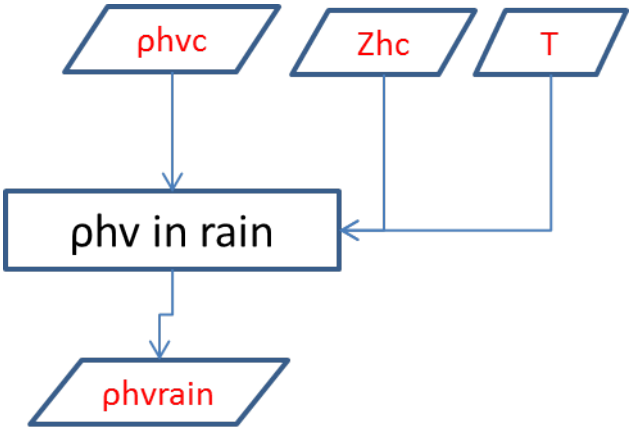

Fig. 8 Flow diagram of the estimation of ρ_{hv} in rain

The freezing level is obtained as follows: If a temperature field is available, all data with temperatures below 0° is filtered out. If a melting layer thickness is defined by the user, for each ray, the altitude of the first filtered gate is determined, the melting layer thickness is subtracted from such altitude and gates above the resultant altitude are also filtered out. If the 3dB beamwidth is also known the beam radius is also subtracted. If no temperature field is available a constant value either given by the user or by default (in such case a warning is issued) is taken as the iso-0° altitude. Table 5 shows the values used for the various radars.

Table 5 Parameters used for the METEOR 50DX and the C-band radars ρ_{hv} in rain estimation.

Keyword	Value	Unit
r_{min}	1000	m
r_{max}	50000	m
Z_{min}	20	dBZ
Z_{max}	40	dBZ
ML_thickness	700	m
Default FZL	2000	m

3.3 Differential reflectivity in moderate rain and precipitation when the radar points vertically

The differential reflectivity in rain provides information of the power balance between the horizontal and vertical channel (both in transmission and reception). According to scattering simulations, at low elevations and moderate rain (i.e. with reflectivity between 20 and 22 dBZ) it should have a mean value of 0.2 dB. When pointing vertically, the differential reflectivity in precipitation should have an average value of 0.0 dB.

The estimation in moderate rain is performed over data fulfilling the following criteria: It is within a range delimited by r_{min} and r_{max}, the reflectivity is within Z_{min} and Z_{max} values, ρ_{hv} is above a minimum threshold ρ_{hv}^{min} (high quality measurement) and the maximum ϕ_{dp} is below a threshold ϕ_{dp}^{max}(low attenuation). The maximum elevation angle is below a certain value θ_{el}. The data must be

below the melting layer according to the procedure discussed in section 3.2. Table 6 summarizes the values used by the various radars.

Table 6 Parameters used for the METEOR 50DX and the C-band radars Z_{dr} in moderate rain estimation.

Keyword	Value	Unit
r_{min}	1000	M
r_{max}	50000	M
Z_{min}	20	dBZ
Z_{max}	22	dBZ
ρ_{hv}^{min}	0.97	-
ϕ_{dp}^{max}	10	°
θ_{el}	20	°
ML thickness	700	M
Default FZL	2000	M

The estimation when the radar antenna points vertically is performed over data fulfilling the following criteria: It is within a range delimited by r_{min} and r_{max}, the reflectivity is within Z_{min} and Z_{max} values, ρ_{hv} is above a minimum threshold ρ_{hv}^{min} (high quality measurement) and the maximum ϕ_{dp} is below a threshold ϕ_{dp}^{max}(low attenuation). Table 7 summarizes the values used by the METEOR 50DX.

Table 7 parameters used for the METEOR 50DX Z_{dr} in precipitation when the antenna is pointing vertically estimation.

Keyword	Value	Unit
r_{min}	500	M
r_{max}	50000	M
Z_{min}	20	dBZ
Z_{max}	40	dBZ
ρ_{hv}^{min}	0.95	-
ϕ_{dp}^{max}	10	°

3.4 Differential reflectivity in snow

As in moderate rain, dry snow (aggregates) can provide useful information on the $\mathrm{Z_{dr}}$ bias since on average it should have a value close to 0 dB albeit with more scatter. Actually it was empirically found to be 0.2 dB.

The estimation in dry snow uses similar parameters to that of moderate rain but in addition the SNR, and optionally the K_{dp} values are constrained. The snow identification is performed using the results of the hydrometeor classification. Table 8 summarizes the values used by the various radars.

Table 8 Parameters used for the METEOR 50DXand C-band radars Z_{dr} in snow estimation

Keyword	Value 50DX	Value C-band	Unit
r_{min}	1000	1000	m
r_{max}	50000	50000	m
Z_{min}	0	0	dBZ
Z_{max}	30	30	dBZ
ρ_{hv}^{min}	0.97	0.97	-
ϕ_{dp}^{max}	10	10	°
SNR_{min}	10	10	dB
SNR_{max}	50	50	dB
θ_{el}	25	25	°
KDP_{max}	Unspecified	Unspecified	°/km
Hydrometeor class	1 (Dry snow)	1 (Dry snow)	-
T_{min}	-50.	Unspecified	°C
T_{max}	-5.	Unspecified	°C

3.5 Estimation of the horizontal reflectivity bias using self-consistency

Theoretically, the drop size distribution (DSD) in rain is fully described by a normalized gamma distribution with 3 parameters:

$$N(D) = N_w f(\mu) \left(\frac{D}{D_o}\right)^{\mu} e^{-\Lambda D}$$

With:

$$f(\mu) = \frac{6}{3.67^4} \frac{(3.67+\mu)^{\mu+4}}{\Gamma(\mu+4)}$$

Where:

$$\Lambda = \frac{3.67+\mu}{D_o} [mm^{-1}]$$

Therefore, only 3 parameters are necessary to fully describe it, N_w, D_0 and μ. Consequently, assuming a fixed μ, only two moments are necessary to describe precipitation but 3 polarimetric variables (K_{dp}, Z_h and Z_{dr}) can be used to estimate the rainfall rate. Therefore, there is a known relation between the 3 polarimetric variables and knowing two the third one can be computed. This fact can be used to estimate the Z_h bias. Considering that K_{dp} does not suffer from any system bias and assuming that Z_{dr} is well calibrated, an estimation of Z_h can be performed from the two and compared with the actual measurement. The difference should be the actual system bias.

In practice we use the technique described in [6]. We pre-compute curves relating Z_{dr} with the ratio K_{dp}/Z_h^{lin} for a particular temperature, elevation and μ. From the measured values of Z_{dr} and Z_h a synthetic K_{dp} is obtained. A synthetic ϕ_{dp} is obtained by integrating over the synthetic K_{dp}. Segments of synthetic ϕ_{dp} are then compared with the measured $\phi_{dp}$and the difference is considered to be the Z_h bias.

Fig. 9 shows the flow diagram of the self-consistency algorithm. A heavy filtration of the dataset is performed to be sure that the highest data quality is used. In the first place a smoothing of Z_{dr} and Z_h is perfomed over a range r_{smooth}. Data with Z_{dr}values outside of the range of values defined by the look up table of $Z_{dr} - K_{dp}/Z_h^{lin}$ value is suppressed. Data with a ρ_{vh} below a threshold ρ_{hv}^{min} and above a maximum ϕ_{dp}^{max} is also suppressed. The segment size for both the synthetic and the measured ϕ_{dp} data has to be of a minimum length r_{cell}^{min} and the ϕ_{dp}excursion has to be between a minimum value $\Delta\phi_{dp}^{min}$(to diminish the influence of phase noise) and a maximum value $\Delta\phi_{dp}^{max}$ (to avoid attenuation). Data has to be well below the melting layer according to the procedure discussed in section 3.2. Table 9 summarizes the values used by the METEOR 50DX.

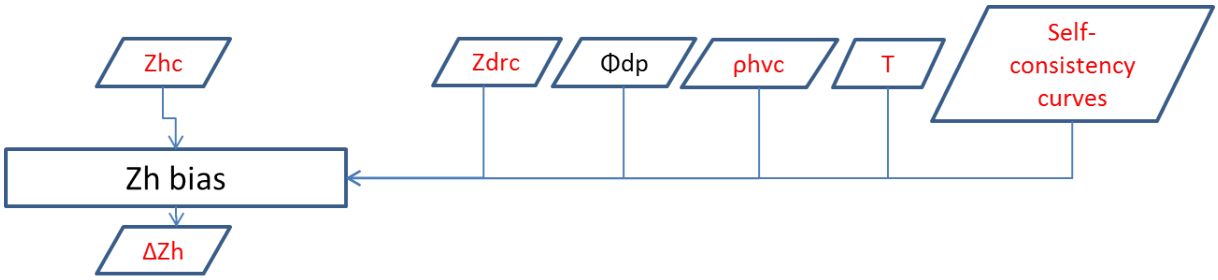

Fig. 9 Flow diagram of the self-consistency algorithm to determine the Zh bias

Although a single value per ray is obtained, for practical reasons the same value is stored in all the gates of such ray.

Table 9 Parameters used to estimate the reflectivity bias of the METEOR 50DX

Keyword	Value	Unit
r_{smooth}	1000	m
ρ_{hv}^{min}	0.92	-
ϕ_{dp}^{max}	20	°
r_{cell}^{min}	1000	m
$\Delta\phi_{dp}^{min}$	2	°
$\Delta\phi_{dp}^{max}$	16	°
ML thickness	700	m
Default FZL	2000	m

3.6 Ground clutter monitoring

If the reflectivity of nearby ground clutter is fairly stable, it can be used to assess the stability of the radar system. The ground clutter monitoring is divided into two steps: the generation of a stable clutter

map and the selection of suitable gates from this map and the reflectivity monitoring proper using this map. In the following these two steps are explained in more detail.

3.6.1 Searching suitable ground clutter gates

To select clutter contaminated range gates first the data is processed daily. The daily processing consists in using the output of the clutter identification to filter the reflectivity so that only identified clutter gates are left. Then the daily occurrence (number of times a particular gate is considered clutter over the day) and the total number of samples obtained during the day is computed and stored in a C/F Radial file. Only clutter-contaminated gates with a reflectivity above 13 dBZ are taken into consideration. In addition, in order to filter out data in rainy conditions, if more than 10% of the gates within the 10 km range used to observe the clutter is labeled as precipitation, the radar volume is not used in the computation.

Once the occurrence has been computed for a significant amount of days, typically one month, the frequency of occurrence of these clutter gates is computed by adding together the occurrence of each day and dividing by the total number of samples. Fig. 10 shows an example of clutter frequency of occurrence map for Weissfluh. The position of gates that have a frequency of occurrence in excess of 95 percent of the time is stored in a csv file.

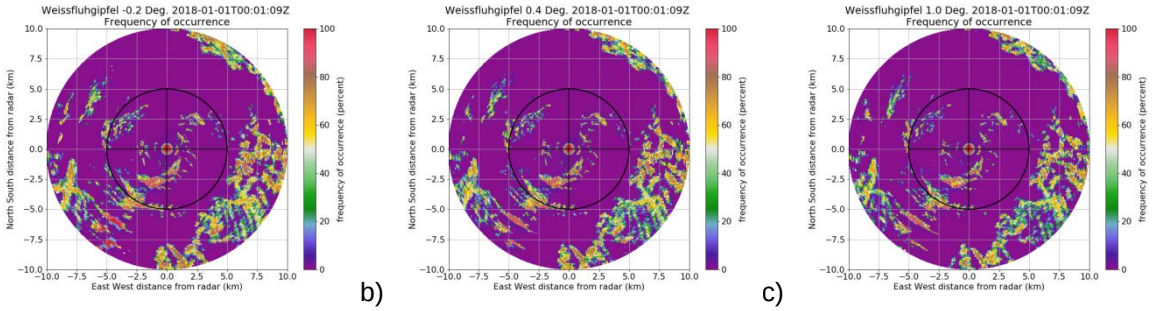

a) b) c)

Fig. 10 Example of ground clutter frequency of occurrence maps for Weissfluh computed over the period 2018.01.01-2018.01.31: a) -0.2° elevation, b) 0.4° elevation, c) 1.0° elevation.

The clutter map has to be recomputed periodically to make sure that the clutter is stable.

3.6.2 Daily monitoring of ground clutter

Once the position of gates with ground clutter is determined following the procedure in section 3.6.1, the histogram of reflectivity values on these gates when the value is larger than 10 dBZ is computed. The 95th percentile of this histogram is considered the clutter reference value. Unless the conditions of the surrounding clutter have changed significantly this value should remain fairly constant for a stable radar.

3.7 Monitoring products

The data used to monitor each polarimetric parameter is input to the process_monitoring function. This function simply obtains the histogram of the data present at each ray. From the monitoring dataset five products can be obtained:

1) A volumetric histogram, i.e. the histogram of all the valid data in a dataset which can be either instantaneous or cumulative along the processing time.

2) A PPI histogram, i.e. the histogram of all the valid data in a particular elevation, also with the possibility of being instantaneous or cumulative.

3) The angular density, which shows the density of valid data as a function of azimuth.

4) The time series of the quantiles of volumetric data as a function of time in the form of a .png plot and a .csv file. If desired, monitoring alarms can be send by email if the current value of the central quantile exceeds a predefined threshold or deviate from the trend of the last precipitation events by a predefined threshold. The trend is computed as an average of the last 10 precipitating events weighted by the number of samples of each event. Table 10 shows the parameters used to issue alarms with the METEOR 50DX.

5) the histogram in a netcdf file with a similar structure as the CF/Radial format that contains the output radar data of Pyrad.

Table 10 Parameters used to define when to issue an alarm using the METEOR 50DX

	ϕ_{dp0}	ρ_{hv} in rain	Z_{dr} in moderate rain	Z_{dr} in vertically pointing	Z_h bias
Min number of daily samples	500000	5000	5000	5000	100
Target value	0.	0.99	0.2	0.0	0.0
Target tolerance	10.	0.04	0.2	0.2	2.0
Trend tolerance	10.	0.02	0.2	0.2	2.0
Number of events in trend	10	10	10	10	10

Fig. 11 shows examples of volumetric cumulative histogram plots obtained by the METEOR 50DX radar in Emmen. Fig. 12 shows an example of angular density at 8.2° for the same date. Large angular variability can be observed which is likely related to the influence of the radome bolts on the signal. Fig. 13 shows the time series evolution of various polarimetric parameters in 2018 for the Dole radar. For the differential reflectivity in rain and system differential phase the quantities represented are the 50% quantile (in blue) and the 25% and 75% quantiles (in red). For the co-polar correlation coefficient in rain, since it has a log-normal distribution and not a Gaussian one (as it can be seen in Fig. 11) the quantities represented are the 80% quantile and the 65 and 95 respectively. The ground clutter plot shows the 95% quantile.

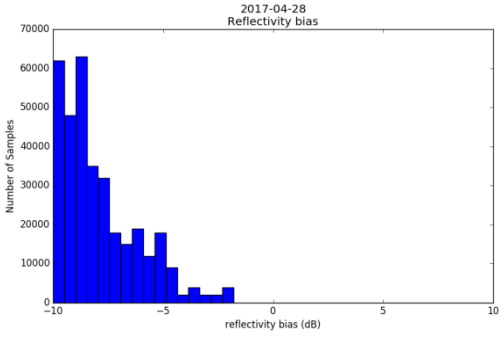

a)

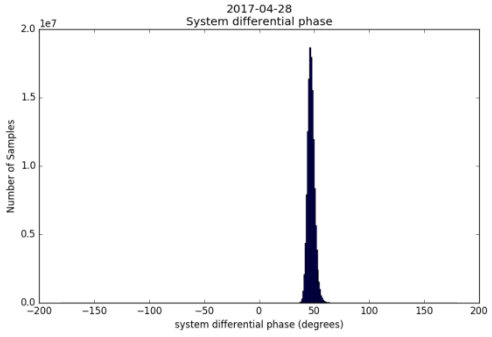

b)

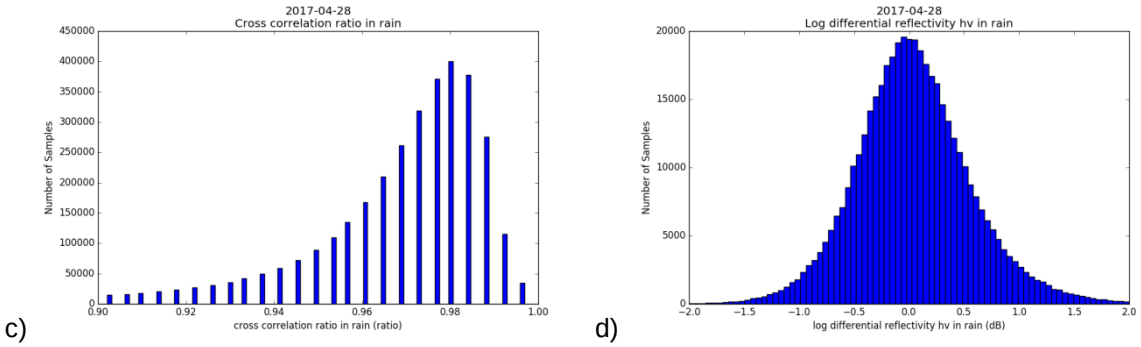

c) d)

Fig. 11 Examples of volumetric histograms obtained from METEOR 50 DX data in Emmen in day 2017-04-28: a) reflectivity bias, b) System differential phase, c) co-polar correlation coefficient in rain, d) differential reflectivity in moderate rain.

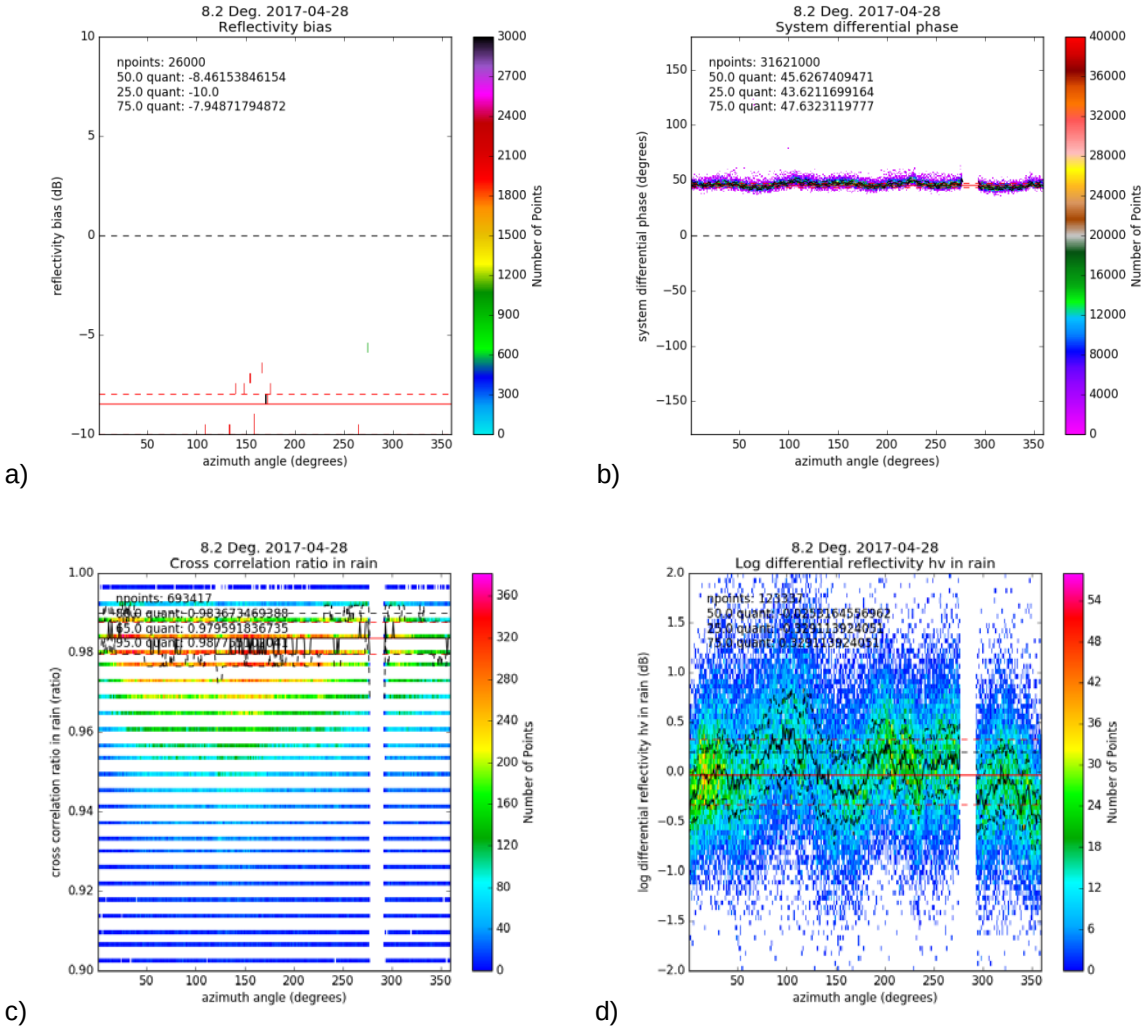

a) b)

c) d)

Fig. 12 Examples of angular density obtained from METEOR 50 DX data in Emmen at elevation angle 8.2° in day 2017-04-28: a) reflectivity bias, b) System differential phase, c) co-polar correlation coefficient in rain, d) differential reflectivity in moderate rain.

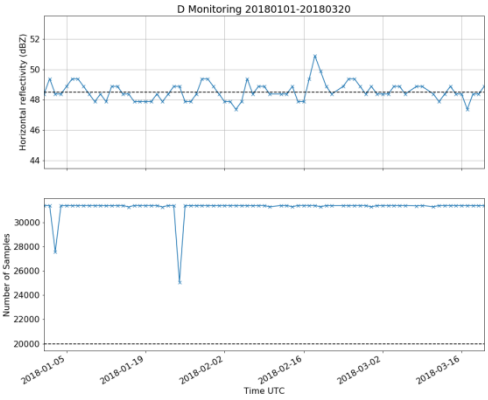

a)

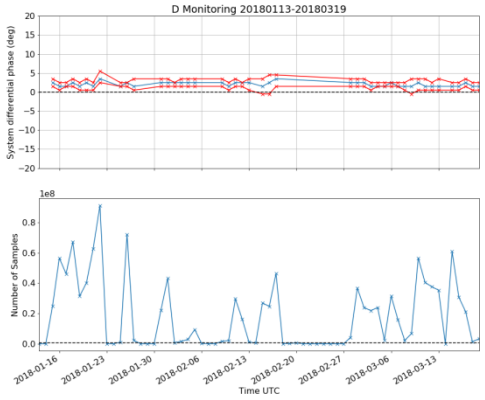

b)

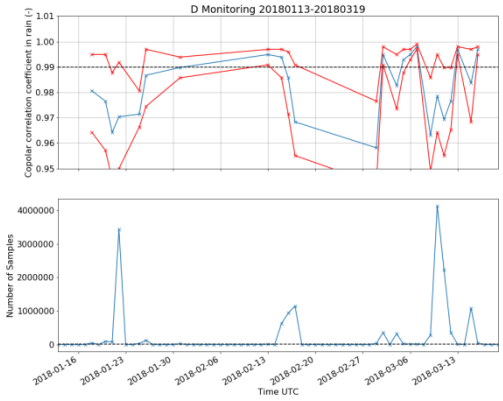

c)

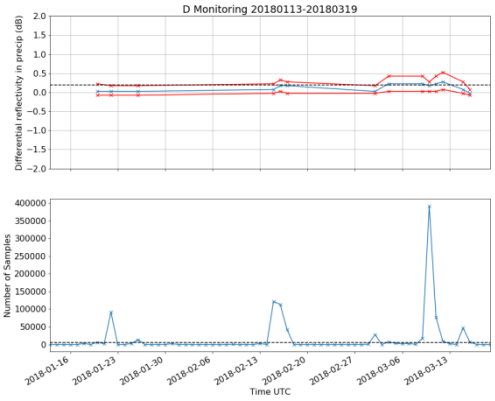

d)

Fig. 13 Example of time series evolution of the polarimetric parameters obtained from data from the Dole radar in 2018: a) ground clutter reflectivity b) System differential phase, c) co-polar correlation coefficient in rain, d) differential reflectivity

Chapter 4 Radar inter-comparison

The radar inter-comparison is performed in three steps:

1. To compute off-line a look up table containing the position in antenna coordinates (azimuth, elevation, range) of the suitable co-located equivolumetric gates.

2. To compute for each radar the hourly reflectivity average (in linear units), the hourly reflectivity weighted differential phase and a flag indicating the conditions of the samples used for the computation of the average (number of gates with clutter, excess of differential phase, number of non-rain gates, etc.)

3. The actual inter-comparison is performed by comparing the hourly average of each radar at the co-located gates obtained from the look up table. Fig. 14 shows the flow diagram of the inter-comparison algorithm.

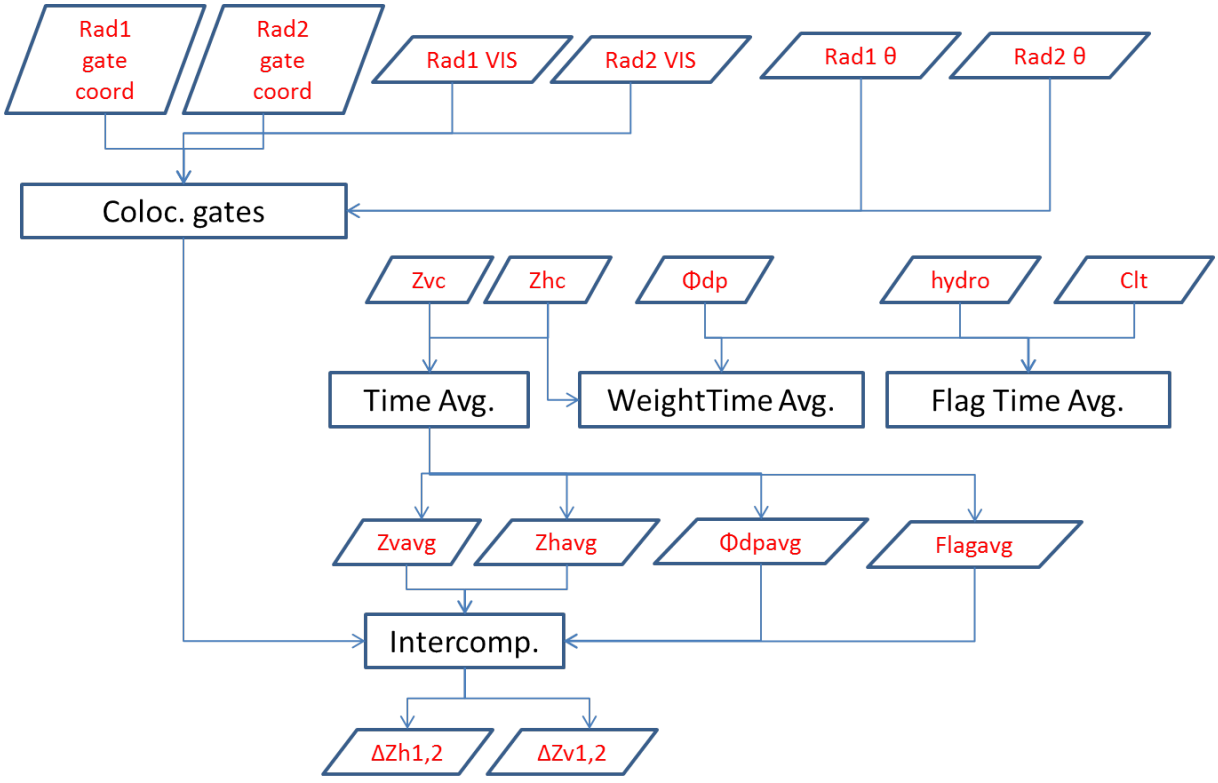

Fig. 14 Flow diagram of the radar reflectivity inter-comparison algorithm

4.1 Searching suitable co-located gates

The search of co-located gates leads to a 3D-boolean matrix where True correspond to co-located gates and False otherwise. It is performed in two steps. In the first place, a region of interest is defined

for each radar. This is performed by first searching for overlapping volumes between the two radars (with a given tolerance in altitude Δh and latitude/longitude $\Delta lat/lon$) with similar volume diameter (within a fixed tolerance ΔD_{vol}) and secondly by filtering out all range gates within the area in one of the radars that do not comply with user-defined conditions. Conditions can be on a minimum visibility VIS_{min}, minimum and/or maximum altitude over the sea level h_{min} and h_{max}, minimum and/or maximum range from the radar r_{min} and r_{max}, minimum and/or maximum elevation angle θ_{el}^{min} and θ_{el}^{max} and minimum and/or maximum azimuth angle per radar. Table 11 shows the parameters used in the search of co-located range gates between the METEOR 50DX in Emmen and the Albis C-band radar and between C-band radars.

In the second step, each range gate identified as within the overlapping region and complying with the conditions in radar 1 is examined to determine whether a complying range gate from radar 2 is co-located (within the aforementioned tolerance on latitude/longitude and altitude). If a co-located gate is not found the Boolean matrix element is set to 0.

The ray and range indexes, elevation, azimuth and range of radar 1 and radar 2 that are found to be co-located are stored in a csv file.

Table 11 Parameters used in the search for co-located gates between the METEOR 50DX and the Albis C-band radar and between C-band radars

Keyword	50DX Value	C-band Value	Unit
Δh	100	250	M
$\Delta lat/lon$	0.005	0.005	°
ΔD_{vol}	100	250	M
VIS_{min}	99	99	%
h_{min}	None	None	M
h_{max}	10000	10000	M
r_{min}	None	None	M
r_{max}	None	150000	M
θ_{el}^{min}	None	None	°
θ_{el}^{max}	20	20	°
az_{min}^{rad1}	None	None	°
az_{max}^{rad1}	None	None	°
az_{min}^{rad2}	None	None	°
az_{max}^{rad2}	None	None	°

In the case of the C-band radars a final step is performed to make sure exactly the same gates are used in the inter-comparison of each reciprocal radar (i.e. Albis compared to Dole versus Dole compared to Albis), whereby of all the gates that have been found to be co-located only those common to both radars are taken into account.

4.2 Temporal averaging

4.2.1 Simple temporal average

The simple temporal average is performed by accumulating radar volumes over time until the desired period is reached. In order to account for possible shifts in range gate positions between one volume and the next a nearest neighbor interpolation taking as reference the position of the first volume in the time series is performed before the accumulation. A counter matrix is used to keep track of the number of samples accumulated. Once the accumulation period is reached, the accumulated volume is divided by the counter matrix and the process is started anew. If desired, logarithmic data (such as reflectivity) can be transformed into-linear prior to the accumulation.

The accumulation period may start at any prescribed time after midnight UTC given by a keyword and the duration of the accumulation (in seconds) can also be prescribed. Table 12 summarizes the parameters used in the hourly reflectivity average

Table 12 Parameters used in the hourly reflectivity average

Keyword	Value	Unit
Period	3600	S
Avg start	0	s from midnight UTC
Lin_trans	True	Boolean

4.2.2 Weighted temporal average

The weighted temporal average works in a similar way as the simple temporal average but in this case the accumulation of the volumes is weighted by the horizontal or vertical reflectivity, which acts as a proxy for the signal intensity. If either the reflectivity volume or the field volume under consideration are not present the data is not accumulated.

The reflectivity data is linearly transformed and multiplied by the field under consideration. A second auxiliary field keeps the accumulation of the reflectivity. Once the accumulation period is reached the reflectivity weighted accumulated field is divided by the accumulated reflectivity. Table 13 shows the parameters used for the estimation of the hourly differential phase average. The reference reflectivity is the horizontal reflectivity corrected by clutter and attenuation.

Table 13 Parameters used in the estimation of the hourly reflectivity-weighted differential phase average

Keyword	Value	Unit
Period	3600	s
Avg start	0	s from midnight UTC

4.2.3 Flag matrix for temporal average

The flag matrix keeps track of the conditions under which the data was accumulated. It looks at three different parameters: ϕ_{dp} in excess of a predefined value ϕ_{dp}^{max}, clutter identified and non-rain precipitation. Each condition is given a counter of up to 99 values so the flag matrix is limited to 99 samples within the accumulation period. These criteria allow the user to make the inter-comparison of the data with a flexible degree of stringency. The ϕ_{dp}^{max} accounts for how tolerant to instantaneous attenuation the user may be, the number of clutter identifications accounts for the tolerance to clutter while the non-rain precipitation allows to select whether only use reflectivity in rain (which it is almost independent from observation angle and frequency) or be more permissive and allow comparison also in solid precipitation.

If ϕ_{dp}^{max} is found +1 is added to the flag matrix, if clutter is found +100 is added and if a precipitating range gate does not contain rain a +10000 is added to the flag matrix.

The ϕ_{dp}^{max} is obtained from the ϕ_{dp} field while the clutter is obtained from the dynamic clutter map generated on the echoID. Wether precipitation is in rain or not it is determined by either checking the hydrometeor classification field or by checking the position of the range gate with respect to the melting layer as discussed in section 3.2. The user defines the behavior by specifying whether the hydrometeor classification field or the temperature field have to be used. If any of the fields necessary to check the conditions is missing the corresponding value is added to all the range gates. Table 14 shows the parameters used for the estimation of the flag matrix. The field used to determine the precipitation phase was the hydrometeor classification field.

Table 14 Parameters used in the estimation of the flag matrix for inter-comparison.

Keyword	Value	Unit
Period	3600	s
Avg start	0	s from midnight UTC
ϕ_{dp}^{max}	60	°

4.3 Inter-comparison of hourly averages

The radar inter-comparison of hourly reflectivity averages (horizontal or vertical) is performed using the precomputed lookup table described in section 4.1. For each element of this lookup table the index of the closest range gate of each radar (within a tolerance) is found. The auxiliary hourly-averaged ϕ_{dp} and flag values of the identified gate are examined. If the two radars have different resolutions, the average reflectivity and weighted-average differential phase of the radar with the higher resolution is downscaled to the resolution of the lowest resolution radar. The flag matrix is also examined so that the maximum value among the range gates used in the averaging for each category is kept. If the reflectivity and the ϕ_{dp} of both radars have a valid value the data is written in a file.

At the end of the examination period, the values that have been written in the file are examined. User defined threshold are used to filter out non-valid data according to: (i) the number of times clutter has been identified $Nclt^{max}$, (ii) the number of occurrences of an excess of instantaneous ϕ_{dp} (ϕ_{dpavg}^{max}), (iii) the number of occurrences of precipitation not defined as rain ($N_{no\_rain}^{max}$) and (iv) maximum value of average ϕ_{dp}(ϕ_{dpavg}^{max}). Values that comply with all the requirements are kept for further analysis. Table 15 shows the parameters used for the inter-comparison between the METEOR 50DX and the Albis C-

band radar in Emmen and between the C-band radars. In such case no discrimination between rain and no rain and values of ϕ_{dp} was performed.

Table 15 Parameters used in the inter-comparison between the METEOR 50DX and the Albis radar in Emmen and the C-band radars

Keyword	Value	Unit
$\Delta\theta_{el}$	0.5	°
$\Delta\theta_{az}$	0.5	°
Δr	100	m
ϕ_{dpavg}^{max}	600	°
$Nclt^{max}$	0	-
$N\phi_{dpexcess}{}^{max}$	100	-
$N_{no\_rain}^{max}$	100	-

4.4 Inter-comparison products

There are two datasets that generate inter-comparison products. The process_colocated_gates dataset takes care of the off-line search for co-located gates and generates a csv file with the list of the co-located gates. Since the dataset is a radar field, it can generate any typical product of a volume scan such as PPI images as shown in Fig. 15.

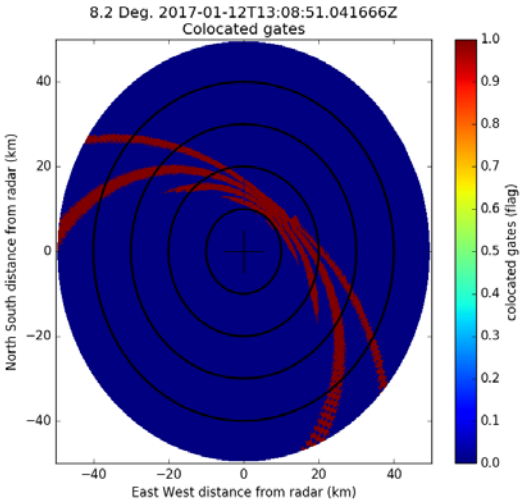

Fig. 15 PPI plot of the METEOR 50DX gates co-located with the C-band Albis radar

The process_intercomp dataset can generate 3 types of products:

1) A csv files containing the position of the valid co-located gates and their values of reflectivity, reflectivity-weighted differential phase and a flag

2) A scatter plot with the values of one radar versus the other and computed scores (number of points, mode bias, median bias, mean bias (computed from the reflectivity in linear units), correlation, intercept point of a slope-1 linear regression, and slope and intercept point of a linear regression).

3) A time-series with the evolution of some of the scores.

Fig. 16 shows an example of scatter plot of the inter-comparison of horizontal reflectivity between the METEOR 50DX placed in Emmen on 25 April 2017 and the Albis radar. In this case it can be seen that the Albis radar was underestimating reflectivity respect to the METEOR 50DX by 2 dB.

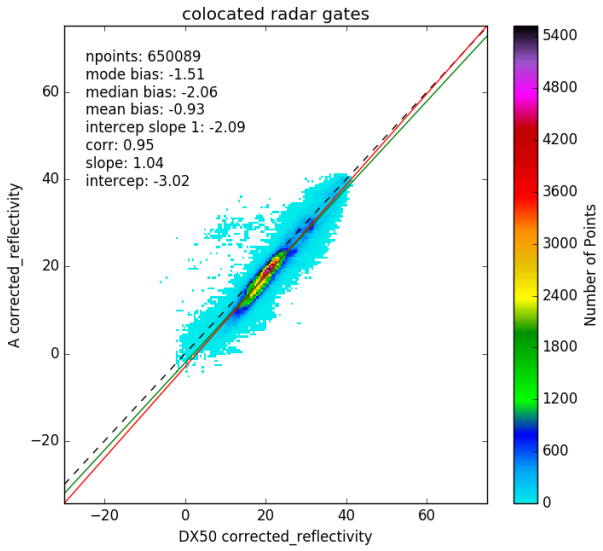

Fig. 16 Inter-comparison of the horizontal reflectivity of the METEOR 50DX placed in Emmen against Albis radar for 25 April 2017.

Fig. 17 shows an example of time series of inter-comparison of the horizontal reflectivity between the Dole and Plaine Morte radars.

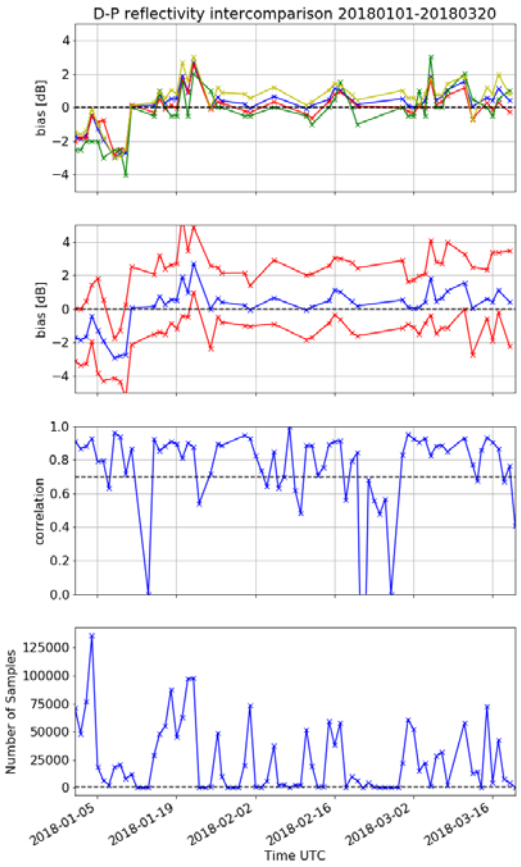

Fig. 17 Time series of the Inter-comparison of the horizontal reflectivity between the Dole and Plaine Morte radars. Plot on top: Blue line: median, red line: mean, green: mode, yellow, intercept of slope one. Second figure: blue line is the median, red lines are the 25th and 75th percentiles.

Chapter 5 Receiver monitoring using sun hits

Since the sun has a precisely known position and its radiating power is accurately measured by astronomic observations and since it is an un-polarized source (hence Z_{dr} is expected to be 0 dB) it can be used to monitor various variables, as well as antenna pointing biases [7], antenna beam width, receiver calibration [8] and imbalances between receiving channels [9]. These checks can be performed by a dedicated sun scan where the radar is pointed towards the sun and a region around it and that data is analyzed. That leads to the most precise results but has the drawback of having to interrupt regular operations. Another method is to identify sun hits obtained during regular operations and make a pool of observations from which to work with. We are describing here the implementation of this second method. This is divided between the identification of sun hits and the retrieval of sun derived parameters.

5.1 Sun hits identification

The first step in the sun hit identification is transform the horizontal and vertical reflectivity into a power (in dBm) at the radome by applying the following formula:

$$P_{rad} = Z - 20\log_{10} r - 2 \cdot Att \cdot r - C - L_{mf} + L_{RX} + L_{rad}$$

Where r is the range in km, Att is the attenuation coefficient (1-way) at the frequency bandwidth of the radar, C is the radar constant, L_{mf} is the match filter losses, L_{RX} are the receiver losses and L_{rad} are the 1-way radome losses. The noise is assumed to be subtracted from the signal. Table 16 shows the value of these parameters for the METEOR 50DX during the Emmen campaign.

Table 16 Values for the conversion of reflectivity into received power at the radome for the METEOR 50DX

Keyword	H Value	V Value	Unit	Comments
Att	0.0120	0.0120	dB/km	
C	82.02	82.13		Taken from file metada. Example value given for shortest pulse
L_{mf}	1	1	dB	
L_{RX}	0.75	0.67	dB	Values in Locarno
L_{rad}	0.3	0.3	dB	

The power at the radome is extrapolated into power at top of the atmosphere in order to take into account the attenuation suffered by the sun signal and expressed in mW:

$$P_{TOA} = 10^{0.1(P_{rad} + Att_{gsun})}$$

Where:

$$Att_{gsun} = Att_g \left(R \sqrt{(\sin\theta_{el})^2 + 2\frac{z_0}{R} + \left(\frac{z_0}{R}\right)^2} - R\sin\theta_{el} \right)$$

Where $z_0 = 8.4$ is the equivalent height of the atmosphere [km] and $R = 4/3 \cdot 6371$ is the effective earth radius [km].

The sun hits identification is performed on a ray basis. For each ray, if the elevation angle is larger than a predefined threshold θ_{el}^{min} the exact sun position with respect to the radar (in antenna coordinates) is determined considering the ray time, the latitude, longitude and altitude of the radar and the refraction of the atmosphere. If the elevation of the sun is above 0° and the ray position is within a window of elevation and azimuth from the radar nominal value $\Delta\theta_{el}$, $\Delta\theta_{az}$ the sun signal is looked for.

Whether there is a sun hit in the received signal it is determined as follows: Valid range gates that are either at a distance further away than r_{min} or have an altitude over sea level larger than h_{min} are examined. If the number of valid range gates is above a certain threshold NB_{min}, the noise-like signal power is estimated using the technique by [10] that filtrates signal from noise and estimates the noise power. If the standard deviation of the estimated noise power is below a certain threshold σ_{max} it is considered a valid sun hit signal. The value of the sun power, standard deviation, number of range gates containing a sun signal, total number of range gates in the segment and a flag array with range gates containing sun signal set as true are returned.

The detection of sun hits in Z_{dr} data is performed as follows: The mean and standard deviation of gates that have been identified as sun hits in both horizontal and vertical channel are computed. If the standard deviation is below a certain threshold σ_{max} it is considered a valid sun hit signal. The value of the mean and standard deviation of the Z_{dr}, the number of range gates containing a sun signal, the total number of range gates in the segment and a flag array with range gates containing sun signal set as true are returned. Table 17 summarizes the parameters used to identify sun hits from METEOR 50DX data.

Table 17 Parameters used for the sun hit identification by the METEOR 50 DX

Keyword	Value	Unit
r_{min}	30000	m
h_{min}	10000	m
NB_{min}	60	-
$\Delta\theta_{el}$	1.5	°
$\Delta\theta_{az}$	1.5	°
θ_{el}^{min}	1.0	°
%bins	10	%
$\sigma(P)_{max}$	1.5	dB
$\sigma(ZDR)_{max}$	1.5	dB

A csv file with all the suspected sun hits (whether a sun signal has been identified or not) is written. The file contains the following information: time in UTC, ray number, number of range gates, radar

elevation and azimuth, sun elevation and azimuth, power in dBm (for H and V channel) and ZDR value, standard deviation, number of range gates identified as sun hits and number of valid range gates in the segment.

The methodology employed has several caveats. In the first place, if precipitation with an homogeneous pattern is present in the ray it may be misidentified as a sun hit. Secondly, if the radar has a poor sensitivity, the sun signal may be partially filtered out by the minimum detectable signal (MDS) threshold. In such case, the sun power is overestimated.

5.2 Sun characteristics retrieval

At the end of the processing period (typically one day) a retrieval is performed from the pool of sun hits retrieved during the day or during several previous days (in the case of the METEOR 50DX 3 days).

The solar flux obtained by the Canadian DRAO (Dominion Radio Astrophysical Observatory) over the period of the pool of sun hits is used as a reference. Since the DRAO reference is obtained at a wavelength of 10.7 cm and given in solar flux units, several transformations have to be performed in order to compare both datasets. In the first place, the DRAO solar flux is converted to the one seen at the wavelength of the radar by using the formula [11]:

$$s_0 = \xi(\lambda)(s_{DRAO} - 64) + sfu(\lambda)$$

Where $\xi(\lambda)$ and $sfu(\lambda)$ are given by Table 19.

On the other hand, each detected sun hit is assigned a DRAO sun flux of reference which is the closest in time to the observation. The last DRAO observation is considered the reference. The power of each sun hit is scaled according to ratio of sun fluxes by adding the scale factor:

$$P^{TOA} += -10\log_{10}\frac{S_0^{rad}}{S_0^{ref}}$$

The sun retrieval is then performed by making a Gauss fit over the pool of valid sun hits. Since the Gauss fit has 5 unknowns a minimum of 5 valid hits is necessary. If desired, a prescribed antenna beamwidth in the azimuth and elevation planes can be imposed. In such case only 3 valid hits are necessary.

For signal power parameters (H or V) the Gauss fit returns the estimated sun power, the standard deviation of the fit, the azimuth and elevation pointing bias, the azimuth and elevation planes beam width, the number of hits used and the parameters returned by the fit. For Z_{dr} the fit returns the estimated sun Z_{dr}, the standard deviation of the fit, the azimuth and elevation pointing bias, the number of hits used and the parameters returned by the fit.

The scanning losses of the antenna and the fact that since the radar is polarimetric only half of the solar flux is observed by it are used to compute the retrieved power on top of the atmosphere:

$$P_{ret}^{TOA} = P_{ret} + l_a + 3$$

Where:

$$l_a = 10\log_{10}\left(l_0\sqrt{\frac{\pi}{4\log_{10}2}}\frac{\Delta c}{\phi_{az}}erf\left(\sqrt{\log_{10}2}\frac{\phi_{az}}{\Delta c}\right)\right)$$

Where ϕ_{az} is the azimuth integration angle and Δc is the sun-convoluted antenna beam width given by:

$$\Delta c = \begin{cases}\Delta c_0(\Delta\theta); \Delta B_{min} \leq \Delta\theta \leq \Delta B_{max} \\ \Delta\theta\end{cases}$$

With Δc_0 obtained as the interpolation of the values given in Table 18.

And:

$$l_0 = \frac{1}{\log_{10}2}\frac{\Delta\theta^2}{\Delta s^2}\left(1 - e^{-\log_{10}2\frac{\Delta s^2}{\Delta\theta^2}}\right)$$

Where $\Delta s = 0.57$ is the apparent diameter of the radio sun [deg].

Table 18 Sun-convoluted antenna beamwidth as a function of the actual antenna beamwidth

ΔB [°]	Δc_0[°]
0.70	0.78
0.75	0.83
0.80	0.87
0.85	0.92
0.90	0.96
0.95	1.01
1.00	1.06
1.10	1.15
1.20	1.25
1.30	1.34
1.40	1.44
1.50	1.54

The next step is to convert the solar power at top of the atmosphere to solar flux units using the following equation:

$$s_0^{ret} = 10^{19}\frac{10^{0.1P_{ret}^{TOA}}}{BA_{eff}}$$

Where:

$$B = \frac{1.2}{\tau}$$

Is the receiver bandwidth and

$$A_{eff} = \frac{g\lambda^2}{4\pi}$$

is the effective area of the receiver antenna. The estimated solar flux is compared to the solar flux from the DRAO reference.

Table 19 Parameters used in the conversion from DRAO solar flux to the radar wavelength

Wavelength λ [cm]	Scale factor ξ	Minimum flux sfu
1	0.67	1980
2	0.68	495
3	0.69	255
4	0.70	170
5	0.71	126
6	0.73	102
7	0.78	88
8	0.84	76
9	0.96	72
10	1.00	68
11	1.00	64
12	0.98	61
13	0.94	58
14	0.90	55
15	0.85	54
16	0.80	53
17	0.78	52
18	0.77	51
19	0.76	50
20	0.75	49
21	0.74	48
22	0.73	48
23	0.72	47
24	0.71	47
25	0.70	47
26	0.69	46
27	0.68	46
28	0.67	45
29	0.66	45
30	0.65	45

5.3 Sun monitoring products

There are several products that can be derived from sun monitoring. After the analysis of each radar volume, if a sun hit is possible, i.e. a radar beam is pointing to the vicinity of the sun position, horizontal and vertical signal power, as well as Z_{dr} can be plotted as a regular volume. Also a binary matrix indicating whether range bins have used to compute the sun power or Z_{dr} value can be plotted. Fig. 18a) shows an example of b-scope plot of the horizontal received power collected in Emmen on 31 December 2017 using the METEOR 50DX . It can be seen a line of homogeneous power at azimuth angle 150° which has been correctly identified as a sun spike in Fig. 18b). After the analysis of each radar volume, information on the collected sun hits can be stored in a csv file.

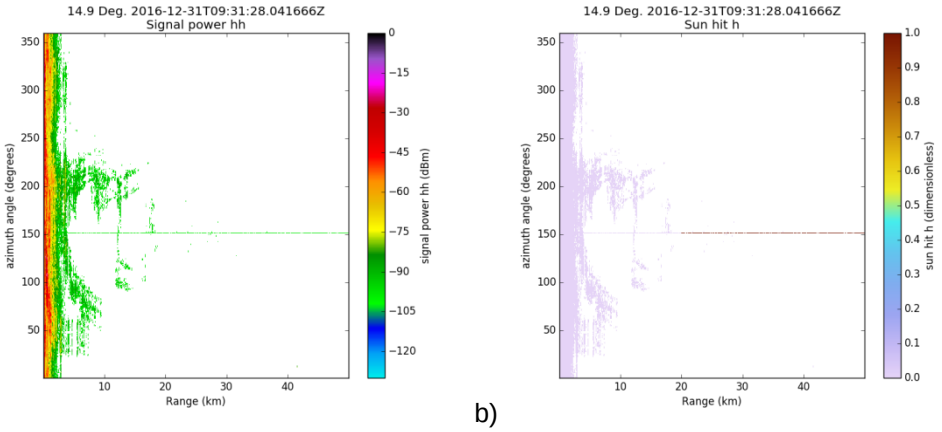

a) b)

Fig. 18 Example of detected sun hit: a) horizontal channel received power, b) range gates used to compute the sun hit power masked in red

At the end of the radar data analysis three different products can be created:

1) A plot of the valid sun hits (horizontal signal power, vertical signal power or Z_{dr}) in a sun-radar azimuth position difference versus sun-radar elevation difference grid

2) A similar plot but with the retrieval (which would show approximately the antenna pattern)

3) The results of the sun retrieval in a text file

4) Time series of the evolution of the various sun retrieval parameters (also with respect to the DRAO reference)

Fig. 19 shows an example of sun hits horizontal power collected over 3 days, from 20 to 22 February 2017 in Emmen using the METEOR 50DX in the radar-sun angle differences plane and its resultant retrieval. Fig. 20 shows an example of the time series with the evolution of various sun retrieval parameters collected by the METEOR 50DX in Emmen. It can be seen that although the data is noisy, a clear trend emerges whereby the receiver was 4 dB higher than the reference until March 2017 and then (after a re-calibration) it went down to 2 dB higher than the reference.

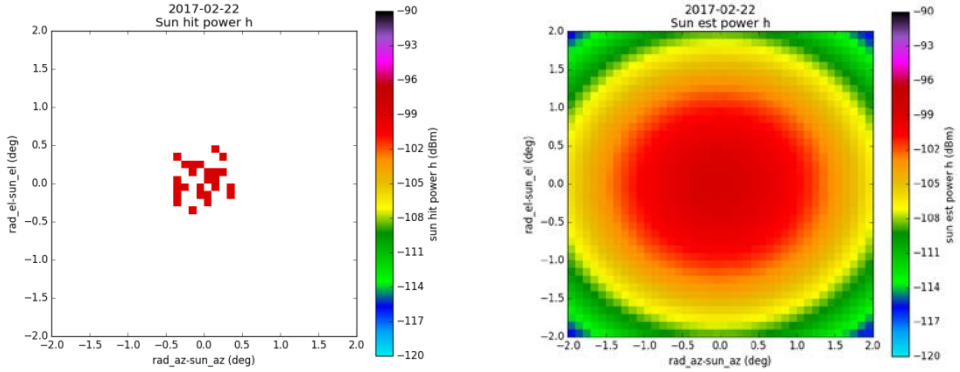

a) b)

Fig. 19 Example of a) sun hits horizontal power in the radar-sun angle differences plane and b) the resultant retrieval

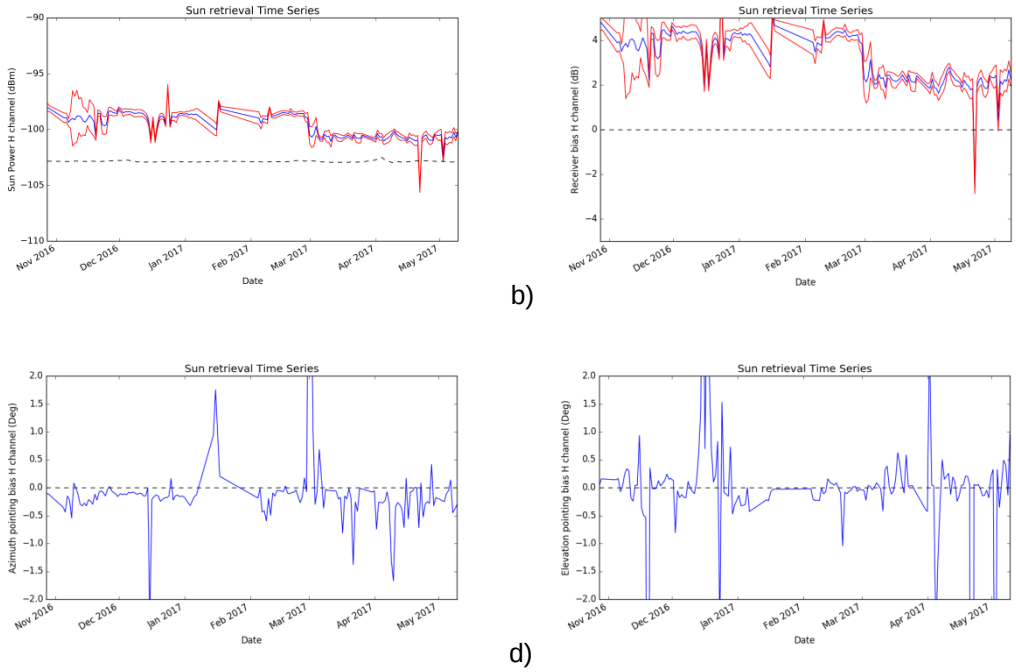

a) b)

c) d)

Fig. 20 Time series of sun parameters collected by the METEOR 50DX in Emmen: a) horizontal received power (mean in blue, standard deviation in red) and DRAO reference (black dashed line), b) bias with respect to DRAO reference, c) azimuth pointing bias of the antenna, d) elevation pointing bias of the antenna

Chapter 6 Conclusion and future work

It is now possible to use Pyrad to monitor operationally the data quality of all the Swiss weather radar systems. There are several tasks that can be performed in order to improve the algorithms:

- C-band radar signal processing should be more sophisticated, particularly what refers to attenuation correction and correcting RhoHV for noise
- The self-consistency algorithm is not working properly. Its implementation and results should be investigated in more detail
- Tests have to be performed of the sun check algorithm with operational C-band data

Chapter 7 References

[1] Gabella, M. and G. Perona, 1998: Simulation of the orographic influence on weather radar using a geometric-optics approach. J. Atmos. Oceanic Technol., 15, 1485–1494.

[2] Testud, J., E. Le Bouar, E. Obligis, and M. Ali-Mehenni, 2000: The rain profiling algorithm applied to polarimetric weather radar. J. Atmos. Oceanic Technol., 17, 332–356.

[3] Besic, N., J. Figueras i Ventura, J. Grazioli, M. Gabella, U. Germann, and A. Berne, 2016: Hydrometeor classification through statistical clustering of polarimetric radar measurements: a semi-supervised approach, Atmos. Meas. Tech., 9, 4425-4445.

[4] Gourley et al. Data Quality of the Meteo-France C-Band Polarimetric Radar, J. Atmos. Oceanic Technol., 23, 1340-1356.

[5] Figueras i Ventura, J., A. Boumahmoud, B. Fradon, P. Dupuy, and P. Tabary, 2012: Long-term monitoring of French polarimetric radar data quality and evaluation of several polarimetric quantitative precipitation estimators in ideal conditions for operational implementation at C-band. Q. J. Roy. Meteor. Soc., 138, 2212–2228.

[6] Gourley, J., A. Illingworth, and P. Tabary, 2009: Absolute calibration of radar reflectivity using redundancy of the polarization observations and implied constraints on drop shapes. Journal of Atmospheric and Oceanic Technology, 26, 689–703.

[7] Huuskonen, A. and I. Holleman, 2007: Determining weather radar antenna pointing using signals detected from the sun at low antenna elevations. J. Atmos. Oceanic Technol., 24, 476–483.

[8] Holleman, I., A. Huuskonen, M. Kurri, and H. Beekhuis, 2010a: Operational monitoring of weather radar receiving chain using the sun. J. Atmos. Oceanic Technol., 27, 159–166.

[9] Holleman, I., A. Huuskonen, R. Gill, and P. Tabary, 2010b: Operational monitoring of radar differential reflectivity using the sun. J. Atmos. Oceanic Technol., 27 (5), 881–887, doi:10.1175/2010JTECHA1381.1.

[10] Hildebrand, P. and R. S. Sekhon, 1974: Objective determination of the noise level in Doppler spectra. J. Appl. Meteor., 13, 808–811.

[11] Tapping, K., 2001: Antenna Calibration Using the 10.7cm Solar Flux, Radar Calibration Workshop RADCAL 2001.

[12] Altube, P., J. Bech, O. Argemí and T. Rigo, 2015: Quality Control of Antenna alignment and Receiver Calibration Using the Sun: Adaptation to Midrange Weather Radar Observations at Low Elevation Angles, J. Atmos. Oceanic Technol., 32, 927-942.